ELSEVIER

Computers and Geotechnics, Vol. 19, No. 2, pp. 153–170, 1996

0266-352X(96)00040-2 0266-352X/96/$15.00+0.00

Identifying Soil Parameters by Means of Laboratory and *in situ* Testing

P. Y. Hicher & A. Michali

Laboratoire de Mécanique: Sols, Structures et Matériaux, CNRS URA 850 École Centrale de Paris, Grande Voie des Vignes, 92295 Châtenay-Malabry Cedex, France

(Received 30 March 1995; revised version received 20 October 1995; accepted 27 October 1995)

ABSTRACT

If the use of in situ *tests for determining soil parameters has been widely developed in the case of empirical relationships or simple models such as the elasticity or perfect plasticity, it is not sufficiently applied when dealing with an elastoplastic model. We present in this paper a methodology for identifying the parameters of an elastoplastic model based on the interpretation of laboratory and* in situ *tests. An inverse method was used to extract several parameters from pressuremeter tests, while triaxial and oedometer tests were used to complement the whole set of parameters. This method has been tested by computing vertical settlements of an embankment on soft clay. The very encouraging results obtained here provided a preliminary validation of this method. Copyright © 1996 Elsevier Science Ltd*

INTRODUCTION

The computation of Civil Engineering structures under working loads, and in particular foundation soil settlements, requires a good knowledge of soil behaviour in a domain of strain very often smaller than 1%. However, in most cases the knowledge obtained from laboratory tests is usually not precise enough, either because of the main effects of remoulding due to the boring (whenever this is possible) on the initial strain characteristics or the lack of precision of the measures in the small strain domain.

Therefore, laboratory results need to be supplemented by *in situ* results. This interaction is currently undertaken in geotechnics in the framework of using constitutive models that describe elasticity or perfect plasticity; however it is not sufficiently applied when dealing with an elastoplastic model.

There is a large variety of *in situ* test methods, all of which have a common characteristic: the realization of non-homogeneous mechanical tests, i.e. tests for which the state of stress and strain in the required material volume varies from one point to another. The interpretation of this variation remains very empirical. Let us mention here Ménard's formulae for the pressuremeter and the use of these formulae for computing settlements and bearing capacities of shallow foundations from pressuremeter test results. The *in situ* results cannot be directly used to determine constitutive models, since they do not produce quantitative relations between stress and strain. In order to obtain such relations, it is necessary to develop inverse methods, that is to claim the constitutive model and to determine its parameters, by computations which take into account all the mechanical (and if necessary hydraulical) factors which condition the test.

These inverse methods have been recently applied to the interpretation of the pressuremeter test [1]; let us note that this test is the most meaningful one among all the tests which concern the *in situ* behaviour of geomaterials for a large class of phenomena from small strain up to failure. The first studies in this field showed that it is undoubtedly illusory to wish through this method to determine all the parameters of a constitutive model that is sufficiently representative of the non-linear behaviour in geomaterials. However, it is possible to determine accurate and meaningful parameters which can account for *in situ* stress–strain behaviour. The present paper defends this approach and proposes a methodology for identifying soil parameters from *in situ* and laboratory tests.

THE CONSTITUTIVE MODEL

We have used HUJEUX's elastoplastic model, [2, 3]. This is a multimechanism model including three deviatory plane mechanisms and one isotropic mechanism. The elasticity is non-linear and it is written as:

$$K = K_i \left(\frac{p}{p_i} \right)^n \text{ and } G = G_i \left(\frac{p}{p_i} \right)^n \tag{1}$$

The yield function (Figs. 1 and 2) of each deviatoric mechanism k (k = 1,...,3), is expressed by:

$$f_k = q_k - p_k \sin\phi \left(1 - b \text{Log} \frac{p}{p_c}\right) g(r_k) \tag{2}$$

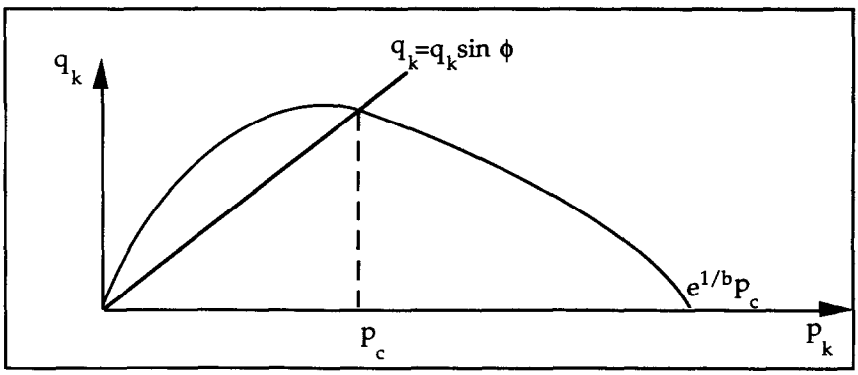

Fig. 1. Yield surface in the (pk, qk) plane for the mechanism k.

we have:

$$p = (\sigma_{zz} + \sigma_{yy} + \sigma_{xx})/3 \tag{3}$$

$$p_k = (\sigma_{zz} + \sigma_{yy})/2 \tag{4}$$

$$S_k = \begin{cases} s_{k1} = \sigma_{zz} - p_k = \dfrac{(\sigma_{zz} + \sigma_{yy})}{2} \\ s_{k2} = \sigma_{zy} \end{cases} \tag{5}$$

$$\text{and } q_k = \| s_k \| \tag{6}$$

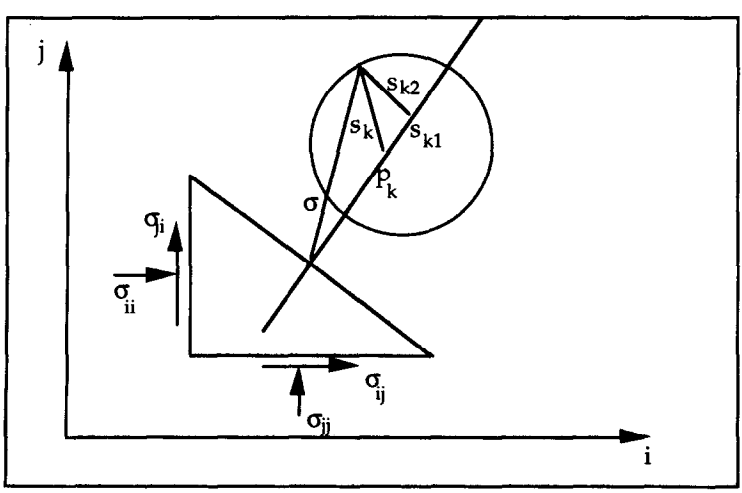

Fig. 2. Rate of stress in (i,j) plane, and Mohr representation for the mechanism k.

where p_c (eqn 2) is the critical stress corresponding to the actual voids ratio; p_c is a hardening variable associated with the volumetric plastic strain; $g(r_k)$ (eqn 2) is a function of the hardening variable r_k, associated with the plastic deviatoric strain of the mechanism k.

We can represent the yield function in a normalised plane $\left(\frac{s_{k1}}{F_{pk}}, \frac{s_{k2}}{F_{pk}}\right)$, Fig. 3

where:

$$F_{pk} = p_k \sin\phi(1 - b\text{Log}\frac{p}{p_c}) \tag{7}$$

$$r_k = 1 - \frac{(1 - r^{el})}{2} \sqrt{\frac{1}{1 + \frac{\epsilon^p_{dk}}{a}}} \tag{8}$$

Its evolution is given by: $dr_k = \lambda_k \frac{(1 - r_k)^3}{a}$, and r^{el} represents the size of the initial elastic domain.

The hypothesis of associated flow in the deviatoric plane of the mechanism k lead to the following relations in the initial HUJEUX's model:

$$g(r_k) = r_k \text{ and } dr_k = \lambda_k \frac{(1 - r_k)^2}{a} \tag{9}$$

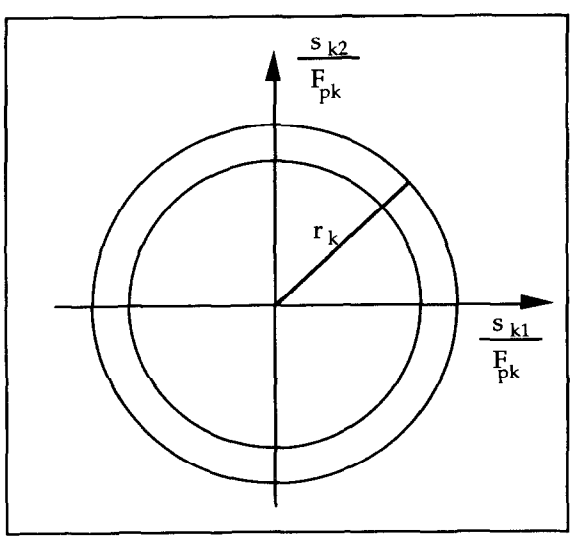

Fig. 3. Presentation of the yield surfaces in the normalised plane.

In order to improve the prediction of the triaxial tests (for both drained and undrained cases) we have retained [4] the following expression for $g(r_k)$:

$$g(r_k) = r_k \left(1 + \sqrt{1 - r_k} \right) \tag{10}$$

b (eqn 7) is a parameter which controls the form of the yield surface in the (pk, qk) plane (Fig. 1). For soft clays, b is generally taken between 0.7 and 1. ϕ (eqn 7) is the friction angle. At critical state the material follows the Mohr-Coulomb failure criterion.
On the other hand the increament of the volumetric plastic strain is:

$$d\epsilon_{vk}^{p} = \lambda_k \left[\sin\psi - \frac{q_k}{p_k} \right] \alpha \tag{11}$$

which generalises the Roscoe's dilatancy law [5]. α is a parameter which regulates the volume change along a deviatoric path; for soft clays, α is close to 1. ψ is the characteristic angle; very often we set: $\psi = \phi$.

The hardening in density is common to the four mechanisms through p_c:

$$p_c = p_{c0} \exp \beta \epsilon_v^p \text{ with } \epsilon_v^p = \sum_{k=1}^{4} \left(\epsilon_v^p \right)_k \tag{12}$$

λ_k is the plastic multiplicator and regulates the magnitude of $d\epsilon_{vk}^{p}$.

Equation (12) defines the position and the slope of the perfect plasticity line in the (e, Log$p$) plane via the initial critical stress p_{c0} defined by means of the initial voids ratio e_0 and the parameter β.
The isotropic mechanism is defined by the yield surface:

$$f_4 = p - dp_c r_4 \tag{13}$$

where d represents (by neglecting the elastic part of the strain) the distance in the (e, Log$p$) plane between the straight line representing the critical state and the parallel one representing the isotropic consolidation; r_4 is a hardening variable associated with the plastic volumetric strain created by the isotropic mechanism.

$$dr_4 = \lambda_4 \frac{(1 - r_4)^2}{c} \tag{14}$$

r^{iso} limits the initial elastic domain of the isotropic mechanism; c controls the slope of the consolidation curve inside the overconsolidated domain.

Kinematic hardening mechanisms have been integrated in the constitutive model in order to reproduce cyclic loading. Our study is however, focused on monotonic loads, we shall not develop here these last mechanisms and the associated parameters.

PARAMETERS OF THE CONSTITUTIVE MODEL

In the case of simulating a monotonic stress path, a set of 13 parameters has to be determined. The model parameters can be divided into the following two groups:

(1) A group of parameters directly measurable from experimental curves: This is the case of the elastic parameters E, ν, (or K, G) (eqn 1), the coefficient of non-linearity n and the parameters r^{el} (eqn 8) and r^{iso} (eqn 14) defining the elastic radii of the deviatoric and isotropic mechanisms. The identification of these parameters is conditioned by the existence of tests for which the strain measurement can be performed in the interval $[10^{-5}, 10^{-4}]$, where the behaviour is really elastic. This condition is not realized for classical triaxial tests or oedometers where the accuracy of the measure is not better than 10^{-3}, [6]; the parameter β is associated with the plastic compressibility and it is expressed as:

$$\frac{1}{\beta} \cong \frac{C_c}{(1 + e_0)2,3};$$

the friction angle ϕ; the parameters $pc0$ (eqn 12) and d (eqn 13) which determine the position of the critical state line in the (e, Log$p$) plane.

(2) a set of numerical parameters, appearing in the different equations, which describe the evolution of the hardening variables; these parameters are a, b, c, α (eqns 7, 8, 11 and 14) and they can only be determined by comparison between numerical and experimental curves, by means of an optimisation procedure.

NUMERICAL SIMULATION OF THE PRESSUREMETER TESTS

The performance of a pressuremeter test calculation by means of a finite element method entails problems of numerical order because we have to solve a coupled hydromechanical (pore pressure and displacement coupled formulation) problem.

Our priority was to study the influence of the model parameters on this special path and to identify those parameters which influence the pressuremeter path calculation in both cases: drained and coupled (pore pressure and displacement coupled formulation) conditions.

The computation under drained conditions allows to determine the parameters characterising the behaviour of the soil skeleton and, in this case, the equilibrium equation, the constitutive law and the boundary conditions are expressed in terms of effective stresses.

In the computation under hydromechanical coupled conditions, with a

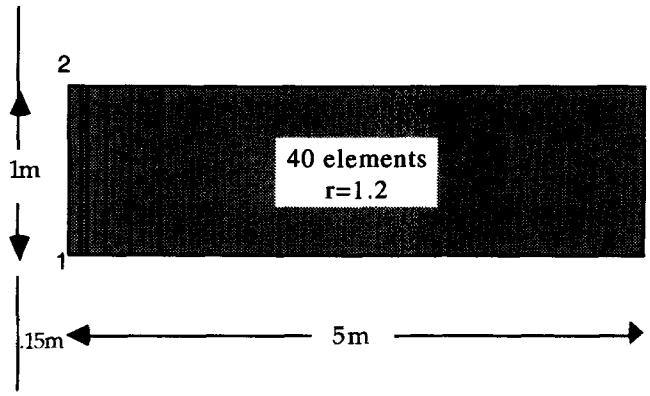

Fig. 4. Spatial discretisation scheme for pressuremeter modelisation.

material of low permeability, as in the case of clays, the pore pressure has been taken into account. The computations were performed under unidimensional and axisymmetric conditions. Several spatial discretisation schemes (Fig. 4) as well as several types of approximation for the deformation and the pore pressure have been examined. Elements with six nodes and six degrees of freedom for the displacements and four degrees of freedom for the pore pressure and four integration points have been chosen [7].

A large variety of meshes have been examined. The choice of the mesh under drained conditions was easily determined. The computation under coupled hydromechanical conditions was more delicate and we finally chose for the modelled domain a zone of 5 m length and 1 m height with 40 elements e_i, $i = 1,....,40$; the length l_i of each element e_i is defined by $l_i = 1{,}2.l_{i-1}$, with $l_1 = 0.0007$m, [7].

In Table 1 the influence of parameters on both drained and coupled (pore pressure and displacement coupled formulation) pressuremeter test is shown [4]:

The essential difference between the drained and coupled pressuremeter tests is the influence of the parameters E and β.

TABLE 1
Influence of parameters on the pressuremeter test calculation in the case of normally consolidated clayed materials

Type of analysis	*Large influence*	*Mean influence*	*Small influence*	*Very small influence*
Drained	ϕ,β,p_{c0}, r^{el},r^{iso}	*b,d*	*E,a*	α,*n,c*
Coupled	ϕ,p_{c0},r^{el},r^{iso}	*E,a,d*	*b*	α,*n,c*,β

β, the plastic compressibility, does not play a major role for the coupled pressuremeter test which is essentially undrained.

E has a weak influence in drained conditions since the majority of the strain is plastic, while E is significant in undrained conditions since it affects the pore pressure increase and, consequently, the effective stresses.

Let us note that we observed the same phenomenon concerning the role of E and β in the triaxial path.

APPLICATION TO THE SITE OF CUBZAC-LES-PONTS

We present now an application of a strategy for the identification of parameters from laboratory and *in situ* tests. We studied the settlement of the embankment *B* foundation at the experimental site of Cubzac-les-Ponts. The embankment *B* was constructed in October 1975 by the LCPC [8]. This embankment has been the object of numerous studies and measures, before, during and after its construction.

On the experimental site, the embankment was built in 1972. In this place the compressible alluvions of Dordogne's valley include:

— a thin layer of vegetal soil of 0.3m,

— a silty clay layer smaller than 2m; this layer is overconsolidated at the surface and alterated by desiccation (the level of the water table varies between the natural level during winter and −1.5 m during summer),

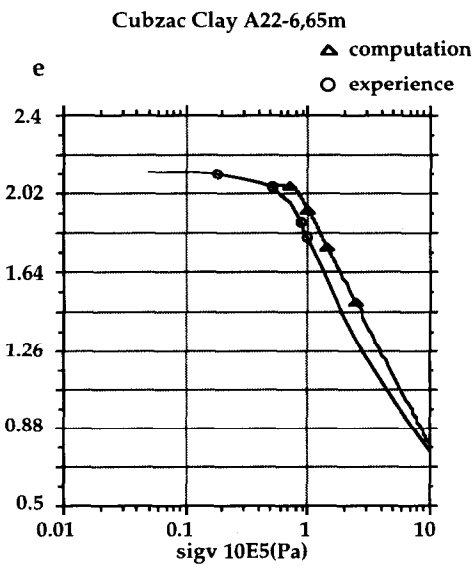

Fig. 5. Oedometer test-horizon at 6.65 m.

— an 8m layer of grey soft clay, more or less organic and slightly over-consolidated.

The substratum consists of a layer of gravels situated at a depth of approximately 9–10 m and of an average height of 5 m, placed on marl or calcareous rocks.

We thus have to determine the parameters of the constitutive model for the several layers of soft clay. For this, we have laboratory tests: oedometer and undrained triaxial tests, as well as *in situ* tests: LCPC self-boring pressuremeter tests.

Use of laboratory tests

These experiments allowed us to directly determine the critical state parameters: ϕ, p_{c0} and d, as well as the plastic compressibility $1/\beta$.

In Fig. 5 we show a comparison between the result from an oedometer test and the theoretical compression based on Eqns (2) and (12) with $\beta = 6{\cdot}5$.

The simulation of undrained triaxial tests (Figs. 6–11) gave a first estimation of the numerical parameters a, b and α, as well as the optimal positioning of the critical state line: $d = 1.5$ and $p_{c0} = 33.10^3$ KPa for $e_0 = 2.13$.

The values of b and α were not modified afterwards:

$b=0.7$, $\alpha=1$.

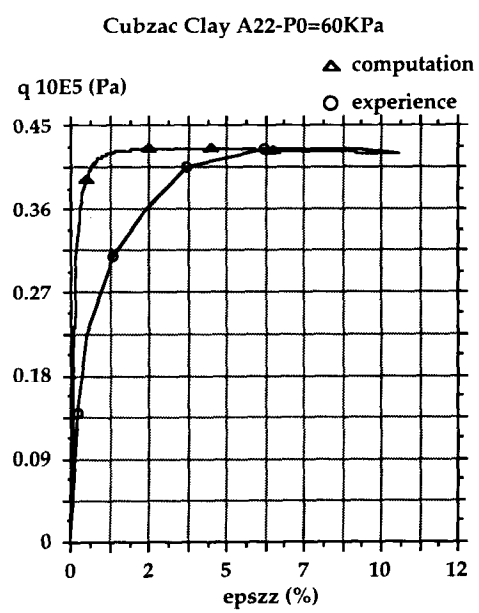

Fig. 6. Undrained test $p_0 = 60$KPa

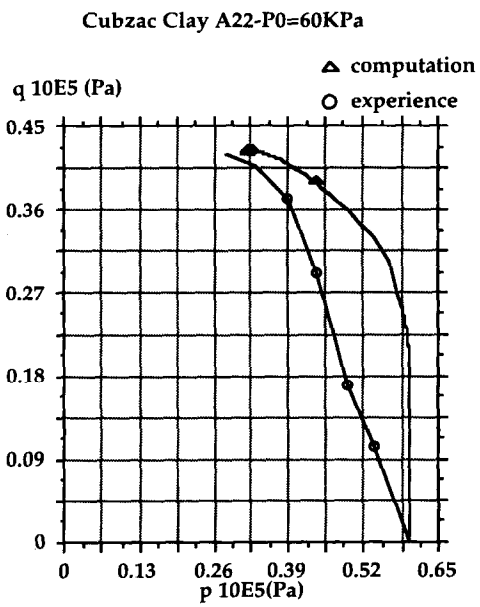

Fig. 7. Undrained test $p_0 = 60$ KPa.

The elastic parameters K, G and n have been estimated by means of standard values obtained in other types of normally consolidated clays for which triaxial tests at small strains were available, [9].

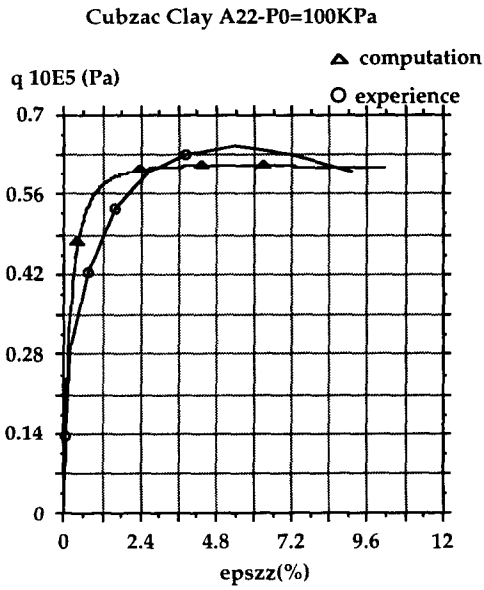

Fig. 8. Undrained test p_0 = 100KPa.

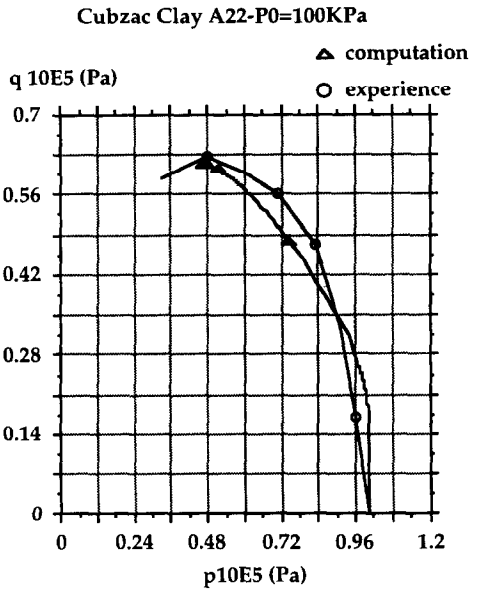

Fig. 9. Undrained test p_0 = 100KPa.

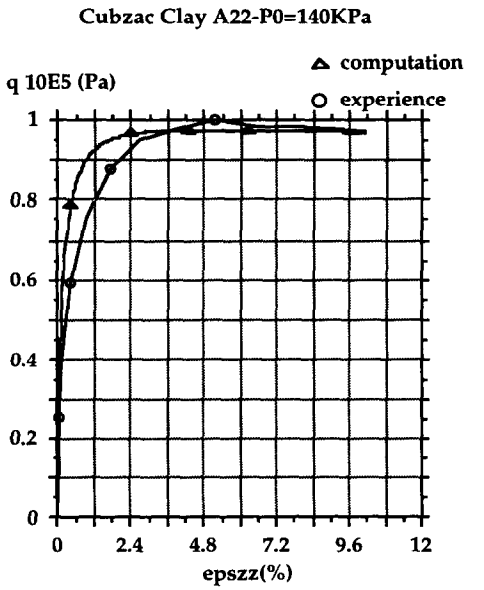

Fig. 10. Undrained test p_0 = 140KPa.

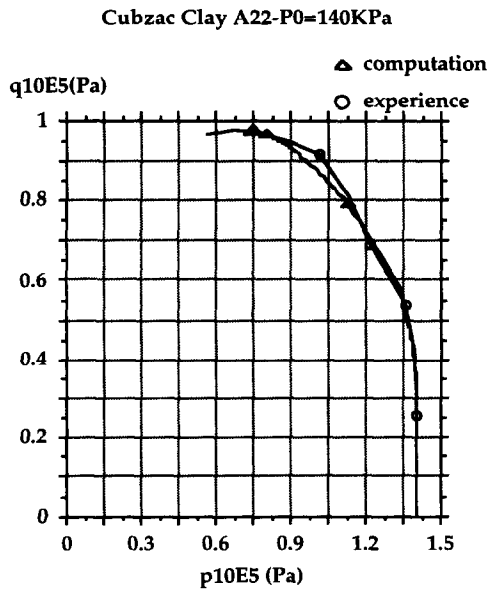

Fig. 11. Undrained test p_0 = 140KPa.

In what follows n and ν have not been modified and have the values: n=0.7, ν=0.3.

The elastic radii are:
r^{el} = 0·001, r^{iso} = 0.6.

Use of pressuremeter tests

The numerical simulation of a pressuremeter test depends on the good knowledge of the initial *in situ* stress state (which is anisotropic).

The lateral stresses at depths where the tests were performed are given from pressuremeter tests; from the values of these stresses we have deduced the corresponding K_0 values.

As an example, we compute K_0 for a test at the depth of 8 m:
The pressuremeter curve starts from $p_0 = 0.88.10^5$ Pa; the water depth is h = 6.7m, so $u = 0.67.10^5$ Pa; we deduce that $\sigma'_h = 0.88.10^5$ Pa–$0.67.10^5$ Pa = $0.21.10^5$ Pa; then: $K_0 = \sigma'_h / \sigma'_{v0} = 0.21.10^5 / 0.46.10^5 = 0.456$.

For 1 m:	For 4 m:
$\sigma'_{v0} = 0.084.10^5$ Pa	$\sigma'_{v0} = 0.30.10^5$ Pa
$u = 0$	$u = 0.14.10^5$ Pa
$\sigma'_h = 0.039.10^5$ Pa	$\sigma'_h = 0.14.10^5$ Pa
$p_0 = 0.039.10^5$ Pa	$p_0 = 0.41.10^5$ Pa
$K_0 = 0.467$	$K_0 = 0.467$

For 5 m:	For 8 m:
$\sigma'_{v0} = 0.33.10^5$ Pa	$\sigma'_{v0} = 0.46.10^5$ Pa
$u = 0.37.10^5$ Pa	$u = 0.67.10^5$ Pa
$\sigma'_h = 0.12.10^5$ Pa	$\sigma'_h = 0.21.10^5$ Pa
$p_0 = 0.49.10^5$ Pa	$p_0 = 0.88.10^5$ Pa
$K_0 = 0.364$	$K_0 = 0.456$

The parameter which plays a crucial role in the numerical simulation of a pressuremeter curve is the initial critical stress p_{c0}, determined from the initial void ratio.

A slight variation of the initial void ratio can result in a significant variation of the p_{c0} value, this fact entailing variations of the maximum stress pL obtained from the calculated pressuremeter curves.

Starting from the simulation of triaxial undrained tests, we have determined the position of the critical state line. The initial void ratio for each pressuremeter test gives the value of p_{c0} for the computation. The distance d between the isotropic line and the critical state line is known; the plastic compressibility β has been determined from the oedometric path.

We have thus concentrated our efforts in the optimisation of the parameters E, a, r^{el}, which influence essentially the elastic and plastic deviatoric deformability. It is natural that these parameters play an important role in the coupled pressuremeter test. The values of E, a and r^{el} were originally estimated by means of standard values obtained by other normally consolidated clays.

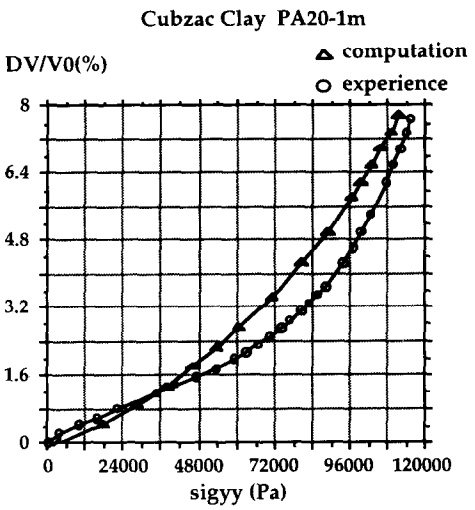

Fig. 12. Pressuremeter test at 1m.

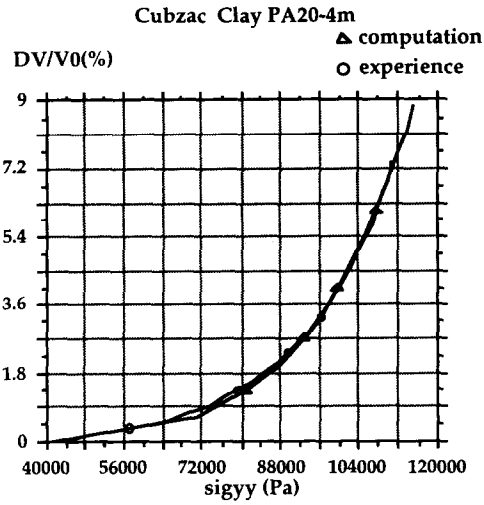

Fig. 13. Pressuremeter test at 4m.

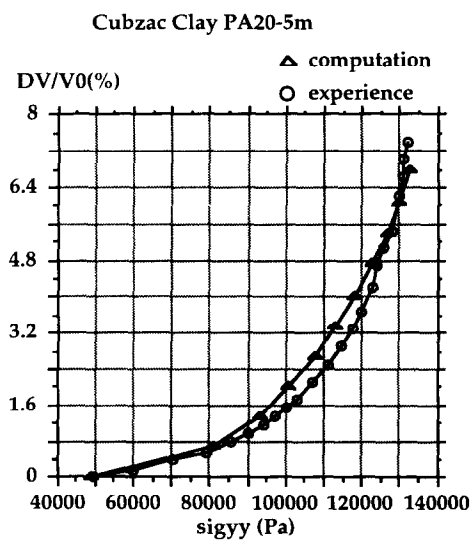

Fig. 14. Pressuremeter test at 5m.

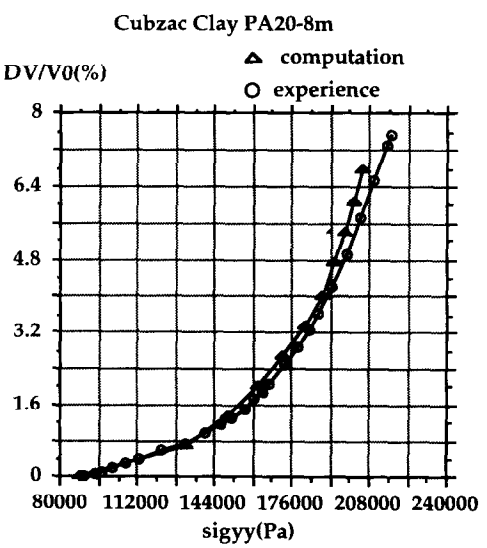

Fig. 15. Pressuremeter test at 8m.

The results of the simulation of the pressuremeter tests are shown in Figs 12–15. The computations were coupled with the following permeabilities:

Pressuremeters	K_v(m/sec)	K_h(m/sec)
at 1 m	5.10^{-9}	$1{\cdot}5.10^{-8}$
at 4 m	3.10^{-9}	$1{\cdot}0.10^{-8}$
at 5 m	3.10^{-9}	$1{\cdot}0.10^{-8}$
at 8 m	1.10^{-9}	$0{\cdot}33.10^{-8}$

As one can see, we obtained a very good reproduction of the experimental results. The retained values are:

$r^{el} = 0{\cdot}001$, $r^{iso} = 0{\cdot}6$, $a = 0{\cdot}0005$,
E(for lm)=24 MPa,
E(for 4m)=63 MPa,
E(for 5m)=65 MPa and
E(for 8m)=80 MPa.

The simulation of the triaxial tests using the set of parameters determined as described above show a fairly important deviation (depending on the experiments) in the initial parts of the curves.

In a second step we could try to improve the numerical simulations of the triaxial paths which appeared stiffer than the experimental curves, but this improvement would create a degradation of the pressuremeter simulations. This compromise between triaxial and pressuremeter simulations did not seem necessary here for the following reasons: (i) the possibility of a remoulding due to the boring which could decrease the initial stiffness of the triaxial samples and (ii) the fact that the viscous nature of the clay was not taken into account in the elastoplastic simulation. The strain rate in triaxial tests was clearly smaller than the one in the pressuremeter tests.

Starting from this study we can propose a procedure (Table 2) for the identification of the parameters. This procedure is based upon the complementarity of the laboratory and *in situ* tests; it consists of determining the

TABLE 2
A systematic way for parameters identification

Experiments	*Identification of parameters*
Undrained triaxial tests	$\phi, e_0, p_{c0}, d, b, \alpha$
Oedometer tests	β
Pressuremeter tests	E, a, r^{el}, r^{iso}

critical state parameters from undrained triaxial and oedometer tests and determining the elastic and plastic strain parameters from pressuremeter tests by means of finite element simulations.

COMPUTATION OF THE SETTLEMENT OF AN EMBANKMENT ON SOFT CLAY

The 9 m soft clay layer under the embankment B was modelled by six layers of distinct mechanical characteristics, the values of which were deduced from both the geotechnical survey [8] and the performed tests are shown in Table 3.

The construction of the embankment was modelled by 10 layers set in 6.3 days.

The computation by means of a finite element method was performed under hydromechanical coupled conditions (pore pressure and displacement

TABLE 3
Mechanical characteristics of the embankment B foundation

Layer	σ'_{v0} *(KPa)*	γ *(KN/m³)*	e_0	ϕ	E	K_v *(m/sec)*	K_h *(m/sec)*
0–1	8·4	16·8	1·65	28	13	5.10^{9}	$1{\cdot}5.10^{8}$
1–2	19·05	14·5	2·3	31	43	5.10^{9}	$1{\cdot}5.10^{8}$
2–4	25·3	14	3·2	31	53	3.10^{9}	$1{\cdot}0.10^{8}$
4–6	34·3	15	2·2	31	65	3.10^{9}	$1{\cdot}0.10^{8}$
6–8	44·3	15	2·1	33	80	1.10^{9}	$0{\cdot}33.10^{8}$
8–9	52·05	15·5	2	33	87	1.10^{9}	$0{\cdot}33.10^{8}$
Emban.	24	21	2	30	20	1	1

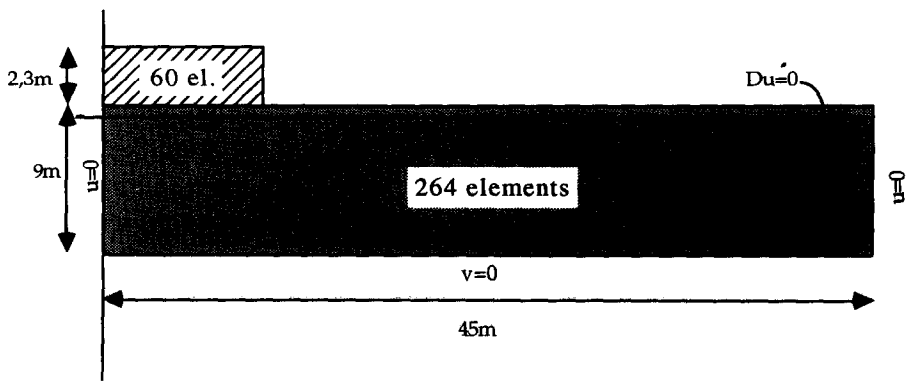

Fig. 16. The embankment B. Modelisation of half of the domain.

coupled formulation) for the foundation and drained conditions for the embankment, in 2D conditions.

The time step was dt = 28000 sec during the construction of the embankment B and dt = 30000 sec once the construction was performed.

The mesh used for the computation represents half of the embankment and of the foundation soil, since the problem is symmetric (Fig. 16). The mesh used for the foundation consisted of 164 quadrilateral elements of eight nodes per element and four integration points and the one of the embankment consisted of 60 quadrilateral elements of eight nodes and four integration points per element.

The computation was performed using GEFDYN [10], a finite element code developed at École Centrale de Paris.

The following boundary conditions have been used:
(1) Null excess pore pressure throughout the surface of the water and the inferior extremity of the mesh in contact with the permeable substratum,
(2) null horizontal displacement on the vertical extremities of the mesh,
(3) null vertical displacement on the inferior extremity of the mesh.

The initial state of the soil is characterized by:
(1) null excess pore pressure everywhere in the domain,
(2) the effective stresses defined by the volumetric weight of the soil, the pore water pressure and, also by the coefficient of earth pressure at rest.

The values of K_v and K_h were deduced from *in situ* self-boring permeameter tests [8], see Table 3 in text on page 166.

A detailed study of the results show that the settlements calculated per layer (Fig. 17) are quite satisfactory with respect to the *in situ* measurement

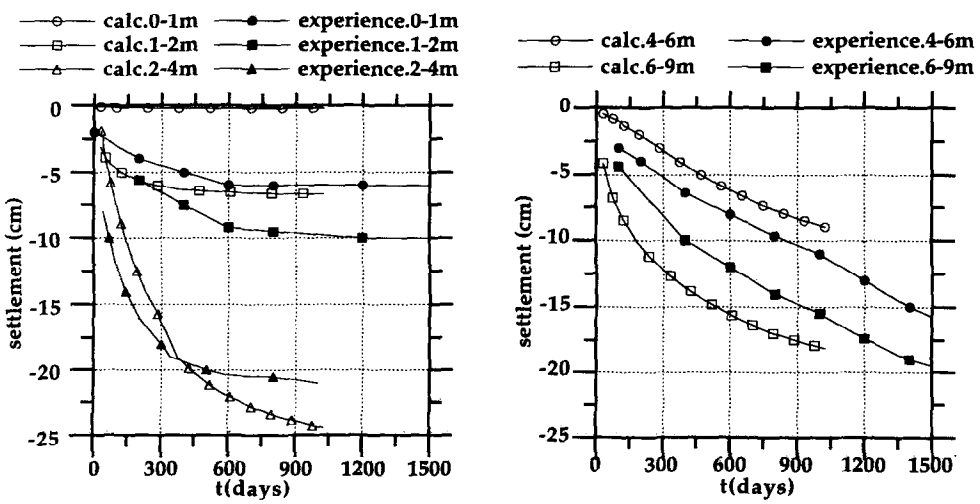

Fig. 17. Settlements per layer.

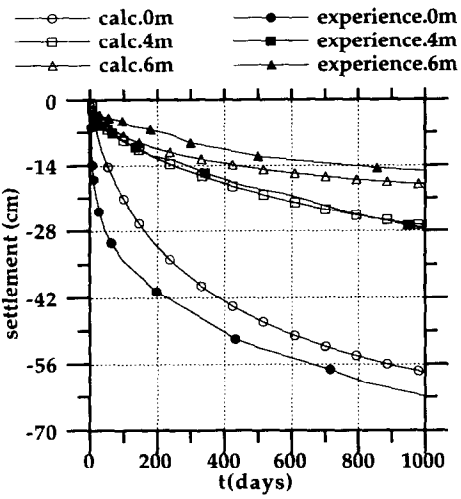

Fig. 18. Global settlements.

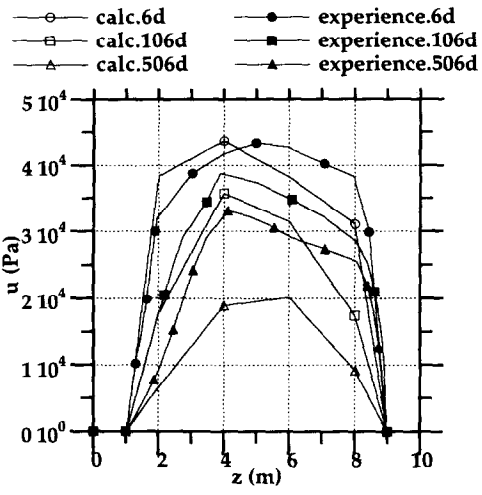

Fig. 19. Excess pore pressure.

concerning the layers from 1m to 2m and from 2m to 4m. The same remark holds for the layers from 4m to 6m and from 6m to 9m.

We have not been able to reproduce the first layer settlement. We have admitted in the computation that the first layer, from 0m to 1m, is drained while, in fact, between the surface and a depth of 1·5m the water table fluctuates. The weathering evolution of this zone was very difficult to take into account in terms of mechanical and hydraulical conditions.

In Fig. 18 the global settlements are shown; one can note that the final settlement, for the node lying under the embankment axis at the soil surface, is almost stabilised after approximately 1000 days because, once the excess pore pressure is dissipated, we have no supplementary settlements. The computed excess pore pressure dissipated faster than in reality (Fig. 19).

After 1000 days we have almost total dissipation of the excess pore pressure and as a consequence, a stabilisation of the computed settlements. The constitutive model used in this study is an elastoplastic one and, therefore, the creep effect was not taken into account. In reality, the measured settlement continued to increase with time up to several years after the construction.

CONCLUSION

We have proposed and validated a methodology (based on both laboratory and *in situ* testing in soft clay) for identifying the parameters of HUJEUX's elastoplastic model.

A parametric study of the pressuremeter test calculation by the finite element method under drained and hydromechanical conditions (pore pressure and displacement coupled formulation) has pointed out the influence of each parameter on the numerical response. Starting from these results we propose to use the pressuremeter results in order to determine by the inverse method a small number of parameters (in our case 3 or 4), chosen among the most influential ones, which have moreover a limited range of values, in accordance with the soil physical characteristics (by means of correlations for example).

In these conditions, the complementary elements given by the interpretation of pressuremeter tests can be very fruitful. We presented an example based on the calculation of the settlements of an embankment on soft clay. Most of the parameters were determined from triaxial and oedometer tests. Those extracted from pressuremeter tests mainly governed the elastic and plastic deformability of the different clay layers that we assumed were more precisely captured by *in situ* self-boring pressuremeter rather than by laboratory tests for which the remoulding due to boring could influence the initial stress–strain relationship.

Very satisfactory results of the calculated settlements at different depths were obtained, which represented a preliminary validation of the method.

More studies are still needed in other cases in order to propose an optimal use of the pressuremeter results according to the type of soil and to the kind of civil engineering structure.

ACKNOWLEDGEMENTS

The authors wish to acknowledge the value of the EDF-SEPTEN fellowship in providing the funding and freedom to conduct this research project.

REFERENCES

1. Cambou, B., Bahar, R., Chapeau, C. & Kazarian, E., Numerical analysis of pressuremeter tests. Application to the identification of constitutive models, *Proc. Second Eur. Speciality Num. Meth. Geotech. Engng*, pp. 369–380, Santander, 1990.
2. Aubry, D., Hujeux, J. C., Lassoudiére, F. & Meimon, Y., A double memory model with multiple mechanisms for cyclic soil behaviour. *Int. Symp. Num. Mod. Geomech.*, Balkema (1982), pp. 3–13.
3. Hujeux, J. C., Une loi de comportement pour le chargement cyclique des sols. In *Genie Parasismique,* (Edited by Davidivici, V.) Presses ENPC pp. 287–302, 1985.
4. Michali, A., Méthode pour l'identification des paramètres d'une loi élasto-plastique à partir d'essais de laboratoire et in-situ-Modélisation numérique du

tassement d'un remblai sur sol compressible. Thèse de Doctorat, Ecole Centrale de Paris (1994).
5. Roscoe, K. H. & Burland, I. B., On the generalised stress-strain behaviour of wet clay. In *Engineering Plasticity*, Cambridge, pp. 535–609, 1968.
6. Biarez, J. & Hicher, P. Y., *Elementary Mechanics of Soil Behaviour-Saturated Remoulded Soils*. A. A. Balkema-Rotterdam-Brookfield, (1994).
7. Modaressi, A. & Michali, A., Choix de la discrétisation en espace pour les problèmes couplés. *Rapport Scientifique du GRECO Géromatériaux*, (1992).
8. Magnan, J. P., Mieussens, C. & Queyroi, D., Etude d'un remblai sur sols compressibles: Le remblai B du site expérimental de Cubzac-les-Ponts. *Rapport de Recherche LPC No 127*, (1985).
9. Hicher, P. Y., Comportement des argiles saturées sur divers chemins de sollicitations monotones et cycliques. Application à une modélisation élastoplastique et viscoplastique. Thèse d'État, Université Paris VI (1985)
10. Aubry, D., Chouvet, D., Modaressi, A. & Modaressi, H., GEFDYN: Logiciel d'analyse du comportement mécanique des sols par éléments finis avec prise en compte du couplage sol-eau-air. *Rapport EdF*/Région d'équipement Chambéry, (1986).